The influence of cooling thimble size on the heat transfer rate in a molten salt reactor residual heat removal system

YANG Zonghao[1], MENG Zhaoming, YAN Changqi[*], and CHEN Kailun

1. *Fundamental Science on Nuclear Safety and Simulation Technology Laboratory, Harbin Engineering University, Nantong Street in Nangang District No. 145, 150001, China (hurricane93@hrbeu.edu.cn)*

Abstract: A thimble-type heat transfer element is an essential part of the drain salt tank in the passive residual heat removal system (PRHRS) of a molten salt reactor (MSR). An experimental loop is designed and built with a single heat transfer element to analyze the heat transfer and flow characteristics. In this research, the influence of the size of a three-layer thimble-type heat transfer element on the heat transfer rate is analyzed. Two methods are employed to obtain the heat transfer rate, with a difference between them of approximately 5%. The gas gap width between the thimble and the bayonet has a large effect on the heat transfer rate. As the gas gap width increases from 1.0 mm to 11.0 mm, the heat transfer rate decreases from 5.2 kW to 1.6 kW. The conduction heat transfer rate accounts for a large proportion in the total heat transfer rate by contrast with the radiation heat transfer rate.

Keyword: molten salt reactor; cooling thimble; natural circulation; heat transfer rate

1 Introduction

With today's rapid development in China, energy shortage and environmental pollution problems are becoming increasingly serious. Because of this, nuclear power has attracted more attention from society because it is clean and highly efficient. However, after the Fukushima accident, individuals worldwide maintain a vigilant and critical perspective toward the development of nuclear power, and China is no exception. Today, nuclear power is an essential energy source because of its prominent advantages. Although the pressure water reactor (PWR) is the most common type of reactor worldwide, it has potential safety risks because of its high-temperature and high-pressure boundaries. In contrast with PWRs, molten salt reactors have the advantages of low pressure, small size, high breeding efficiency, and little residual radioactivity [1].

The molten salt reactor concept was put forward in the early 1960s. In 1965, Oak Ridge National Laboratory (ORNL) successfully designed and built the molten salt reactor experiment (MSRE) [2,3], and successfully operated it for four years. By the end of 1969, it had fully demonstrated the feasibility of using molten fuel and a molten heat transfer medium [4]. Research into MSRs was set aside in 1972, and since then the U.S. has focused on the liquid metal fast breeder reactor (LMFBR). Japan has studied the FUJI series of molten salt reactors beginning in the 1980s and continuing to today.

Beginning in the 21st century, MSR studies have gradually made their way back into the internationally agenda because the MSR is proposed as the generation IV nuclear reactor. The U.S. proposes a fluoride salt-cooled high-temperature reactor (FHR), which has many things in common with a MSR. The FHRs use solid nuclear fuel, cooled with low-pressure molten fluoride. The goal of FHRs is to generate large amounts of electric power and high-temperature process heat reliably and economically [5]. After the Fukushima accident, Japan accelerated the pace of research process on the FUJI series of molten salt reactors. FUJI is a thermal reactor that uses the fuel FLiBe mixed with U/Pu/Tu. The moderator is graphite, which doesn't need changing during the reactor core's lifetime [6]. To achieve the efficient transmutation of the transuranium elements in the light water reactor spent fuel, Russia proposed to use transuranium elements instead of the U-Pu circle as a nuclear fuel to build a molten salt actinide recycler & transmuter (MOSART) [7]. France is developing a molten salt fast reactor (MSFR), in which the fuel circle uses two launching modes, the ^{233}U launch and the transuranium elements launch [8]. The technological and experimental studies of both MOSART and

Received date: June 6, 2017
(Revised date: June 14, 2017)

MSFR have goals of decreasing the generation of highly toxic radioactive waste while simultaneously generating the electric power. China is also putting efforts into a molten salt reactor. The Shanghai Institute of Applied Physics and Chinese Academy of Sciences plans to build a 100MW thorium molten salt reactor (TMSR) by 2030.

Nomenclature			
A	area (m^2)	τ	record time (s)
C_p	specific heat at constant pressure (kJ/(kg K))	Φ	heat transfer rate (W)
D	equivalent diameter (m)	Subscripts	
F	enhancement factor	*a*	acceleration resistance
fr	friction factor	*ba*	bayonet
G	mass flux (kg/(m^2 s))	*bi*	bayonet inner wall
h	heat transfer coefficient (W/(m^2 K))	*bo*	bayonet outer wall
H	enthalpy (W)	*co*	conduction
k	thermal conductivity (W/(m K))	*cw*	condensed water
P	pressure (Pa)	*f*	friction resistance
Pr	Prandtl number	*fi*	feed tube inner wall
Re	Reynolds number	*fo*	feed tube outer wall
S	suppression factor	*fu*	furnace
T	temperature (K)	*g*	gravity resistance
x	dryness fraction	*hs*	heat section
X	angle factor	*poor*	poor boiling
X_{tt}	Martinelli parameter	*ra*	radiation
Greek symbols		*rc*	rising channel
ΔP	pressure drop (Pa)	*ti*	thimble inner wall
ΔT_{sat}	inner wall superheat of thimble, T_{bi}-T_{sat} (K)	*to*	thimble outer wall
ε	emissivity of pipe wall	*tp*	two phase
μ	dynamic viscosity (Pa s)	*sat*	saturation
υ	specific volume (m^3/kg)	*sd*	steam dome
σ	surface tension coefficient (N/m)	Superscripts	
σ_1	Stefan-Boltzmann constant	$'$	liquid phase
		$''$	gas phase

The residual heat removal system is an important component of an MSR [9, 10]. After the molten salt reactor shuts down, the fuel salt is drained into the drain salt tank through a frozen valve. Two primary plans exist to cool the fuel salt in the drain salt tank: external cooling of the drain salt tank and internal cooling using heat transfer elements. The representative method for the external cooling plan is the reactor external vessel cooling (REVC), which is a mitigation strategy for a severe accident. For a reactor core meltdown, the decay heat of melt can be removed from the bottom head by two-phase natural circulation in the reactor external vessel cooling channel, and the in-vessel retention (IVR) is realized. Currently, this cooling method has been applied practically in the AP1000 and APR1400 [11].

For the external cooling plan design for the molten salt reactor, in reference to the REVC method of the AP1000, the drain salt tank is placed in the pool and the heat is removed by natural convection of the water outside the drain salt tank. However, if this method is employed, the fuel salt at the center of the drain salt tank may not be sufficiently cooled due to the tank's very large volume, and the continuous generation of decay heat may make the temperature of the molten salt rise to a level greater than the fuel salt temperature limit. The drain salt tank is also equipped with a heater to prevent the fuel salt from solidifying during the heat removal process. When the heater runs, the pool-type residual heat removal system remains in operation, working against the efforts to maintain the molten salt temperature. Another disadvantage is that the heat dissipation power can be difficult to control.

There are several plans for internal cooling, one of which is to use a thimble-type heat transfer element designed by ORNL, which was successfully operated for four years. There have also been some new

designs for the residual heat removal systems in recent years. One such design, developed by WANG Chenglong *et al.*, immerses the drain salt tank in a secondary coolant molten salt pool, and NaK heat pipes are placed across the drain salt tank to transfer the heat from the fuel salt in the drain salt tank to the secondary coolant molten salt [12]. Another design, developed by Ishiguro T *et al*., consists of the drain tank, a closed water circuit and an air cooler. 30cm diameter heat transfer pipes pass vertically through the drain salt tank. The water in the heat transfer element goes through the drain salt tank and transfers heat to the air cooler. At the outlet of air cooler the collected cooling water circulates back to the drain salt tank [6]. In the current research, we will use a furnace to simulate the high temperature environment of molten salt. The design of WANG Chenglong *et al*. is relatively complicated, containing fuel salt and NaK liquid alloy. The dimensions of the heat transfer element designed by Ishiguro T. *et al*. are relatively large, which makes furnace design challenging. Further, both the designs of WANG Chenglong *et al*. and Ishiguro T. *et al*. are purely theoretical. By contrast, the ORNL design has been operated successfully for four years, which fully proves the feasibility of a thimble-type heat transfer element. Therefore, in the current research, the experimental heat removal loop is based on the ORNL design. In the ORNL residual heat removal system, the cooling thimbles are directly inserted into the drain salt tank to remove the sensible heat and decay heat of the fuel salt. The schematic of the residual heat removal system designed by ORNL is shown in Fig. 1. From the figure, it is evident that this type of residual heat removal system is not passive. If the entire system loses electricity, the water pump will shut down, and the heat of the high temperature water in the condenser cannot be removed, resulting in failure of the residual heat removal system.

2 Experimental natural circulation loop

An experimental natural circulation loop is designed and built to simulate the heat transfer process in the PRHRS of an MSR. The experimental loop is designed with a single cooling thimble based on the ORNL design. A schematic of the test loop is shown in Fig. 2. This experimental loop removes the redundant part of ORNL's design, and the new, compact design can remove residual heat passively. The entire system consists of two natural circulation loops, one of which is the heat transfer element itself. The other natural circulation loop is the steam dome and the pipeline between the steam dome and the condenser.

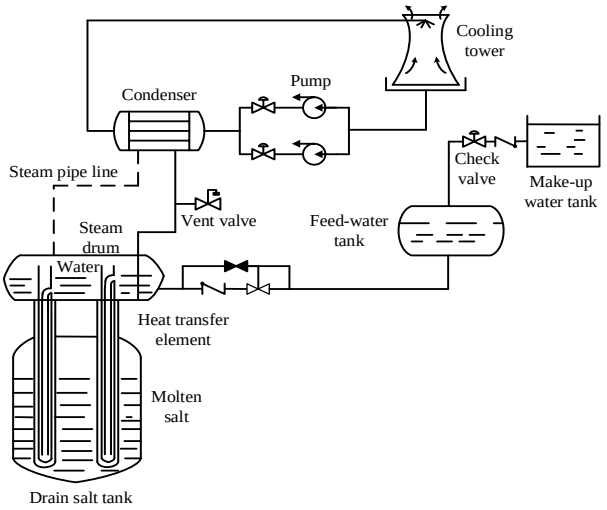

Fig. 1 The schematic of the MSR residual heat removal system.

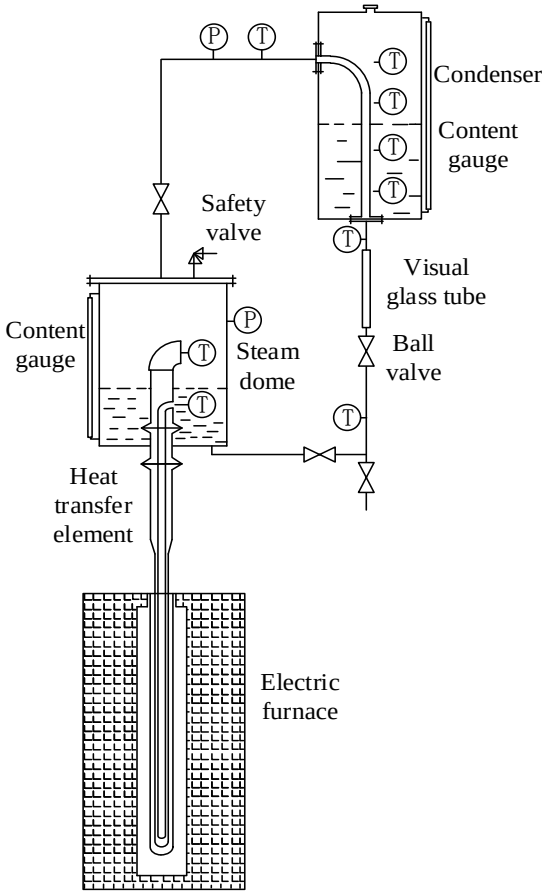

Fig. 2 Schematic of the test loop.

In this experiment, a high-temperature electric furnace is employed to simulate the high-temperature environment of the molten salt. The heat transfer element consists of three concentric pipes. There is a thimble outside the bayonet. Without the thimble, there would be a very large temperature difference and consequently high thermal stress on the bayonet, which is located between the coolant water and the high temperature molten salt. This structure can effectively avoid accidents (such as an explosion) that can occur when there is only one single thimble, which can be damaged by corrosion when high-temperature molten salt touches the coolant water directly. The structure of the heat transfer element and the thermocouple arrangements are shown in Fig. 3. The dimensions of the cooling thimble in both this experimental loop and the ORNL MSR are shown in Table. 1.

Table 1 Original dimensions of the heat transfer element.

Structure		Dimensions
Cooling thimble	Feed tube	12.70 mm×1.19 mm, 2.97 m in length
	Bayonet	25.60 mm×1.5 mm, 3.10 m in length
	Thimble (a), (b), (c)	31.88 mm×1.15 mm, 38.08mm×1.18 mm, 45.16 mm×1.47 mm, 1.395 m in length
	Heating section	1.395 m
Cooling thimble designed by ORNL [13]	Feed tube	12.70 mm (0.5 inch), 1.994 m and 2.096 m in length
	Bayonet	25.40 mm (1 inch), 2.149 m in length
	Thimble	38.10 mm (1.5 inch), 1.968 m in length
	Heating section	1.689 m

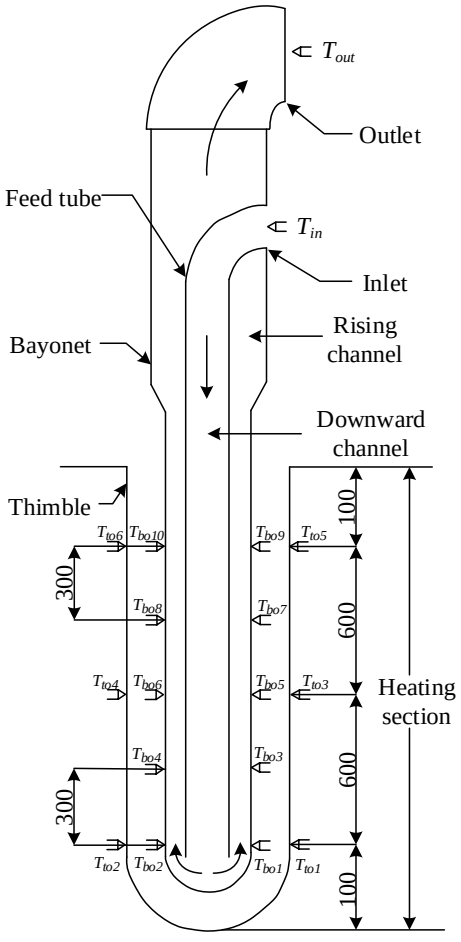

Fig. 3 Schematic of the cooling thimble with thermocouple locations.

In the heat transfer element of the natural circulation loop, the water coolant flows down through the feed tube (downward channel). When it reaches the bottom, it will turn and flow upwards through the rising channel due to the heat from the thimble. The driving force of the system depends on the density difference between the downward channel and the rising channel. The water in the cooling thimble absorbs heat and generates steam. The steam then passes through the steam dome and flows into the condenser where it is condensed and then flows back to the steam dome. The previous steps describe the primary heat removal process in this experiment.

Prior to the experiment, the water in the steam dome and condenser are heated to boiling. Next, the non-condensable gas in the experimental loop is drained out. The experiment will not begin until the water temperature in the condenser and the system pressure stabilizes. The steam flow rate is measured indirectly by measuring the amount of condensed water. When the system stabilizes, the ball valve, located below the glass tube will be shut down. The steam generated from the heat transfer element is condensed into water in the condenser. The condensed water is then received in the glass tube and the liquid level variation is recorded over time.

3 Calculating the heat transfer and flow

In addition to the experimental loop, a self-compiling program was developed to study the change in cooling thimble heat transfer rate with specific detailed pipe diameters. The locations of the wall temperature measurements and the pipe diameters are shown in Fig. 4. The simplified calculation processes for the heat transfer rate and mass flow rate are shown in Fig. 5. The thermal resistance schematic of the cooling thimble is shown in Fig. 6. For the calculation of heat transfer and flow processes, first, assume an initial heat transfer rate Φ_1 and an initial superheat $\Delta T_{sat,1}$ of the feed tube inner wall. The heat transfer rate Φ_2 and superheat $\Delta T_{sat,2}$ are obtained through a series of calculations shown in the figure. It is necessary to note that Φ_1 and $\Delta T_{sat,1}$ are the initial assumption values, Φ_2, $\Delta T_{sat,2}$, and others are the iterative values during the iteration process. The specific calculation equations for Φ are shown in Eqs. (12-14) in section 4.2 of this paper. Φ_1 and $\Delta T_{sat,1}$ will be changed until Φ_1 is equal to Φ_2 and $\Delta T_{sat,1}$ is equal to $\Delta T_{sat,2}$. Assume an initial mass flow rate M. By doing so, the two-phase flow pressure drop will be obtained. Then, the initial M will be revised until the sum of the four types of pressure drop is equal to the driving pressure head P_d. Finally, the heat transfer processes and the flow processes are coupled together to obtain the final heat transfer rate and mass flow rate.

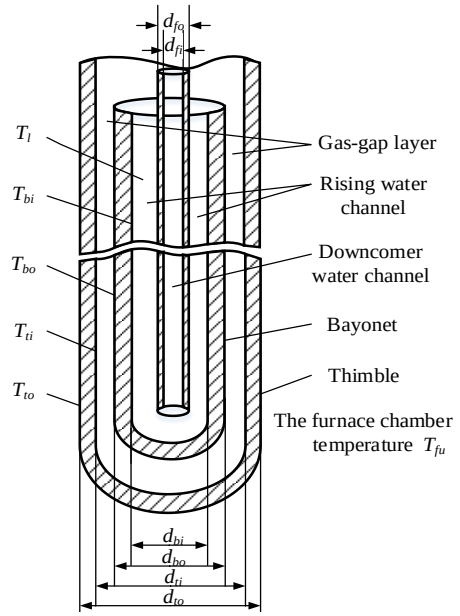

Fig. 4 The locations of wall temperature measurements and pipe diameter.

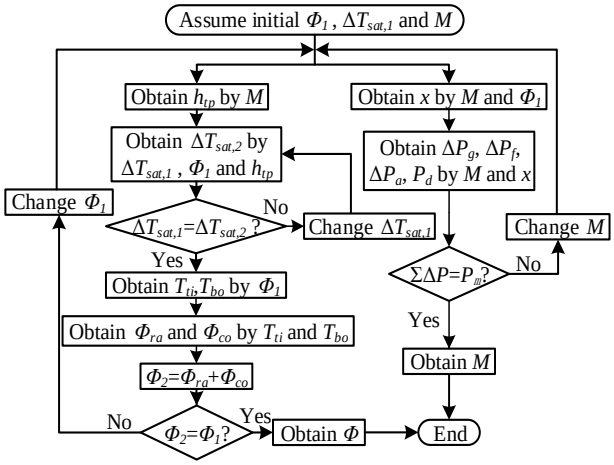

Fig. 5 The calculation process for heat transfer rate and mass flow rate.

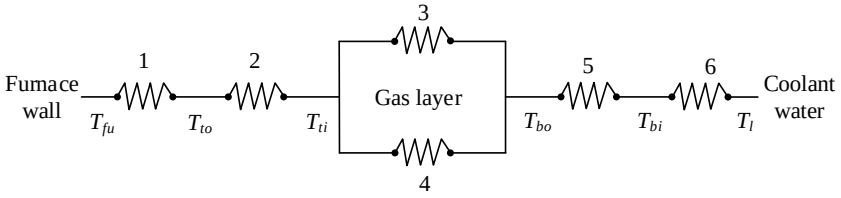

1, Conduction and radiation thermal resistance 2, Thimble thermal resistance 3, Radiation thermal resistance 4, Conduction thermal resistance 5, Bayonet thermal resistance 6, Convection thermal resistance

Fig. 6 The thermal resistance schematic for the cooling thimble.

To calculate the heat transfer coefficient, the classical Chen formula [14] is applied for saturated and subcooled flow boiling. The Chen formula is listed as follows:

$$h_{tp} = h_{pool} \cdot S + h' \cdot F \tag{1}$$

$$h_{pool} = 0.00122 \cdot (k')^{0.79} C_p^{0.45} (\upsilon'')^{0.24} \Delta T_{sat}^{0.24} \Delta P_{sat}^{0.75} \cdot (\sigma^{0.5} (\mu')^{0.29} (H'' - H')^{0.24} (\upsilon')^{0.49})^{-1} \tag{2}$$

$$h' = 0.023 \cdot (Re')^{0.8} (Pr')^{0.4} (k'/D_{rc}) \tag{3}$$

$$S = (1 + 2.53 \cdot 10^{-6} (Re')^{1.17})^{-1} \tag{4}$$

$$F = 2.35 \cdot (1/X_{tt} + 0.213)^{0.736} \tag{5}$$

$$F = 1 \tag{6}$$

h_{pool} is the pool boiling heat transfer coefficient, and h' is the liquid phase convective heat transfer coefficient. The parameter S is called the suppression factor which accounts for the fact that the pool boiling correlations over-predict the actual nucleate boiling. The parameter F is called the enhancement factor which accounts for the enhancement of forced convection heat transfer because of the existence of vapor. For subcooled flow boiling, the effect of the gas-phase is negligible compared to that in saturation boiling. Eq. (5) is then rewritten as Eq. (6) [15].

To calculate the two-phase flow pressure drop, a homogeneous flow model is employed. Several assumptions are made for the calculation. First, in the rising channel, the vapor and liquid have equal linear velocities. Second, the thermodynamic equilibrium is attained between the vapor and liquid phases. Third, the friction factor fr_{tp} is assumed equal to that which would have occurred had the total flow been assumed to be all liquid. Additionally, the friction factor fr_{tp} is evaluated using a mean two-phase viscosity μ_{tp} in the normal friction factor relationship. The primary calculation equations are given by Eqs. (7-11). Besides ΔP_f, ΔP_g and ΔP_a, the friction pressure drop through the non-heating section and the pressure drops through the enlargement, the bend *etc*. are similar to them, and are not listed in there.

$$\Delta P_f = 2 \cdot fr_{tp} G_{rc}^2 L_{ba} \upsilon' / D_{rc} \cdot [1 + (\upsilon'' - \upsilon')x / 2\upsilon'] \quad (7)$$

$$fr_{tp} = 0.079 \cdot (G_{rc} D_{rc} / \mu_{tp})^{-0.25} \quad (8)$$

$$1/\mu_{tp} = x/\mu'' + (1-x)/\mu' \quad (9)$$

$$\Delta P_g = \ln[1 + x(\upsilon'' - \upsilon')/\upsilon'] \cdot g L_{ba} / [x(\upsilon'' - \upsilon')] \quad (10)$$

$$\Delta P_a = G_{rc}^2 \cdot (\upsilon'' - \upsilon') \cdot x \quad (11)$$

4 The analysis of heat transfer characteristics near the cooling thimble

4.1 Temperature distribution in the thimble tube

The cooling thimble is heated by a high-temperature electric furnace. With PID technology, the furnace temperature in each segment can be adjusted automatically, and the temperature can be controlled within 2°C. The furnace temperatures are set at 800°C, 750°C, 700°C, 650°C, 600°C and 550°C. The axis thermocouple distribution on the thimble tube is shown in Fig. 3. Figure 7 shows the average values of T_{to2}, T_{to4} and T_{to6} at approximately 5 minutes when the furnace temperature is stable. L_{hs} is the heating section length of the thimble and L is the distance of the thermocouples from the thimble bottom. The points of each shape correspond with a furnace temperature T_{fu}. As shown in Fig. 7, the furnace temperature is higher than the outer wall temperature by approximately 100°C, which demonstrates that there is a large temperature difference in the radial direction of the furnace chamber.

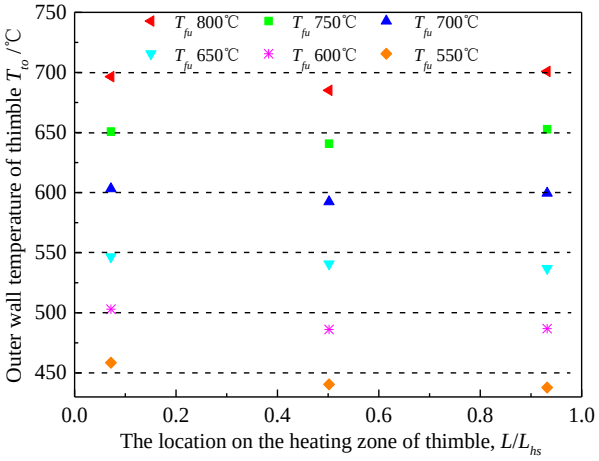

Fig. 7 The distribution of outer wall temperature at the corresponding furnace temperature.

For better accuracy of the temperature measurements, the pipe wall is grooved with keyways along its axial direction. A photograph of the keyway and the soldered dot is shown in Fig. 8(a). The sizes of the keyways are 5 cm in length, 2 mm in width, 0.5 mm in depth and the sheathed K-type thermocouples are buried into the keyways by silver brazing. This method is effective in avoiding the phenomenon that the measured wall temperature is slightly higher than the true wall temperature due to the radial temperature gradient in the furnace chamber. As shown in Fig. 8(b), in the method of traditional electric fusion welding, the thermocouples are welded on the pipe wall in the radial direction. Even when the welding is done correctly, there will be approximately 1 mm of the thermocouple which is perpendicular to the pipe wall. When the furnace temperature is 700°C, there will be about a 500°C temperature difference in the air layer between the thimble and the bayonet. The air temperature at position A will slightly higher than that

at B. However, the thermocouple measurements at position A will be similar to that at B, and at position B, the thermocouple measurements which are simply welded on the pipe wall would be higher than the air temperature at the same position. The reason for this phenomenon is that the thermocouple at position A prefers to transfer heat to the thermocouple at position B through the thermocouple itself rather than through the air due to its low thermal resistance. Location pins welded on the pipe wall are used to keep the pipes concentric.

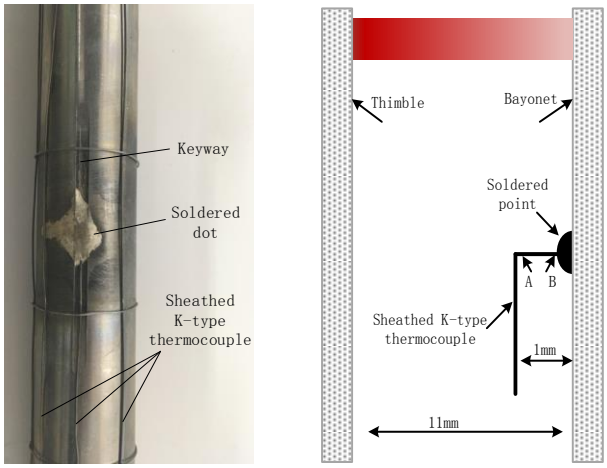

(a) Method employed in the experiment (b) Traditional method

Fig. 8. A photograph and a schematic of welding methods

4.2 The change in heat transfer rate for different gas gap widths and different temperatures

Φ_{total} is the total heat transfer rate which is introduced from furnace and is removed by water in the bayonet. In this section, two methods are employed to calculate Φ_{total}. The first method is to calculate Φ_{co} and Φ_{ra} between the bayonet and thimble. The total heat transfer rate obtained from the first method is simplified as $\Phi_{total,1}$. T_{bo} and T_{ti} are used as the boundary conditions to calculate $\Phi_{total,1}$. In the second method, the total heat transfer rate $\Phi_{total,2}$ is calculated by the latent heat of vaporization. Since heat is preserved sufficiently in the experimental loop, the heat loss through the pipeline is neglected and the heat brought in by the furnace is considered to be equal to the heat removed by the vaporization of saturated water. The vapor flow rate can be obtained from the condensed water, and the detailed method is illustrated in the section on the experimental facility.

In the calculation process, the outer wall of the thimble is divided into five parts. The temperature of each part is considered to be uniform, measured by the thermocouples in the each part. The equations to calculate $\Phi_{total,1}$ and $\Phi_{total,2}$ are shown in Eqs. (12-15). In the equations, τ is the time of steam condensation, and L_{cw} is the height of the condensed water.

$$\Phi_{ra}=\frac{\sigma_1(T_{ti}^4-T_{bo}^4)}{A_{bo}(1-\varepsilon_{bo})/\varepsilon_{bo}+1/A_{bo}X_{bo,ti}+A_{ti}(1-\varepsilon_{ti})/\varepsilon_{ti}} \quad (12)$$

$$\Phi_{co}=\frac{2\pi kL_{hs}(T_{ti}-T_{bo})}{\ln(d_{ti}/d_{bo})} \quad (13)$$

$$\Phi_{total,1}=\Phi_{ra}+\Phi_{co} \quad (14)$$

$$\Phi_{total,2}=\frac{\pi D_{cw}^2 L_{cw}\cdot(H''_{sat}-H'_{sat})}{4\tau\cdot\upsilon'} \quad (15)$$

To calculate of Φ_{ra} and Φ_{co}, the angle factor $X_{bo,ti}$ is considered to be equal to 1 because the bayonet is surrounded by the thimble. Due to the large influence of pipe wall emissivity on the radiation heat transfer, the emissivity of the pipe wall was measured in Automatic Detection in Process Control Systems Research Institute, Harbin Institute of Technology. The results show that T_{bo} is fairly stable, and the average emissivity ε_{bo} of the bayonet outer wall for different wavelengths is 0.25. However, T_{ti} changes dramatically, and the change in emissivity with temperature can be represented as ε_{ti}=0.0005×T-0.1. The changes in heat transfer rate with T_{to} at different gas gap width are shown in Fig. 9.

Figure 9 (a), (b) and (c) indicate that there is little difference between the two methods of obtaining the heat transfer rate. The average difference between them is approximately 5%, and the largest difference is within 10% which demonstrates that the parameter measurement and calculation are relatively accurate. Moreover, as shown in Fig. 9 (a), the conduction heat transfer rate occupies a relatively larger proportion (more than 75%) of the total heat transfer rate when the gas gap width is 2.0 mm. In contrast, the radiation heat transfer rate occupies a relatively larger proportion (approximately 60%) of the total heat transfer rate when the gas gap width is 8.31 mm. The reason for this is that when the gas gap width is narrow, the heat resistance is small, and the conduction heat transfer rate is very large. Increasing the gas gap width results in the increase of heat resistance and the

decrease of the conduction heat transfer rate. At the same time, an increase in the radiation heat transfer area results in an increase in the radiation heat transfer rate.

As shown in Fig. 9 (d), the heat transfer rate at different temperatures decreases when the gas gap width increases. The heat transfer rate at a gas gap width of 2.0 mm is observably larger than that at the 5.05 mm and 8.31 mm gas gap widths. This occurs because the gas gap width is very narrow and the air heat resistance is very small, which makes the conduction heat transfer rate very large. The decrease in the gas gap width will also reduce the radiation heat transfer area, which reduces the radiation heat transfer rate. However, on the whole, the influence of gas gap width on conduction heat transfer rate is larger than that on radiation heat transfer rate, resulting in the decrease of total heat transfer rate as gas gap width increases. Moreover, it can be seen from Fig. 9 (d) that there is little difference in the heat transfer rate between gas gap widths of 5.05 mm and 8.31 mm, with an average difference of only 5.05 mm and 8.31 mm is only 10%. As shown in Fig. 9 (b) and (c), the conduction heat transfer rate occupies a larger proportion at the 5.05 mm gas gap width, but the radiation heat transfer rate occupies a larger proportion at the 8.31 mm gas gap width. On the whole, there is little difference in the total heat transfer rate between them.

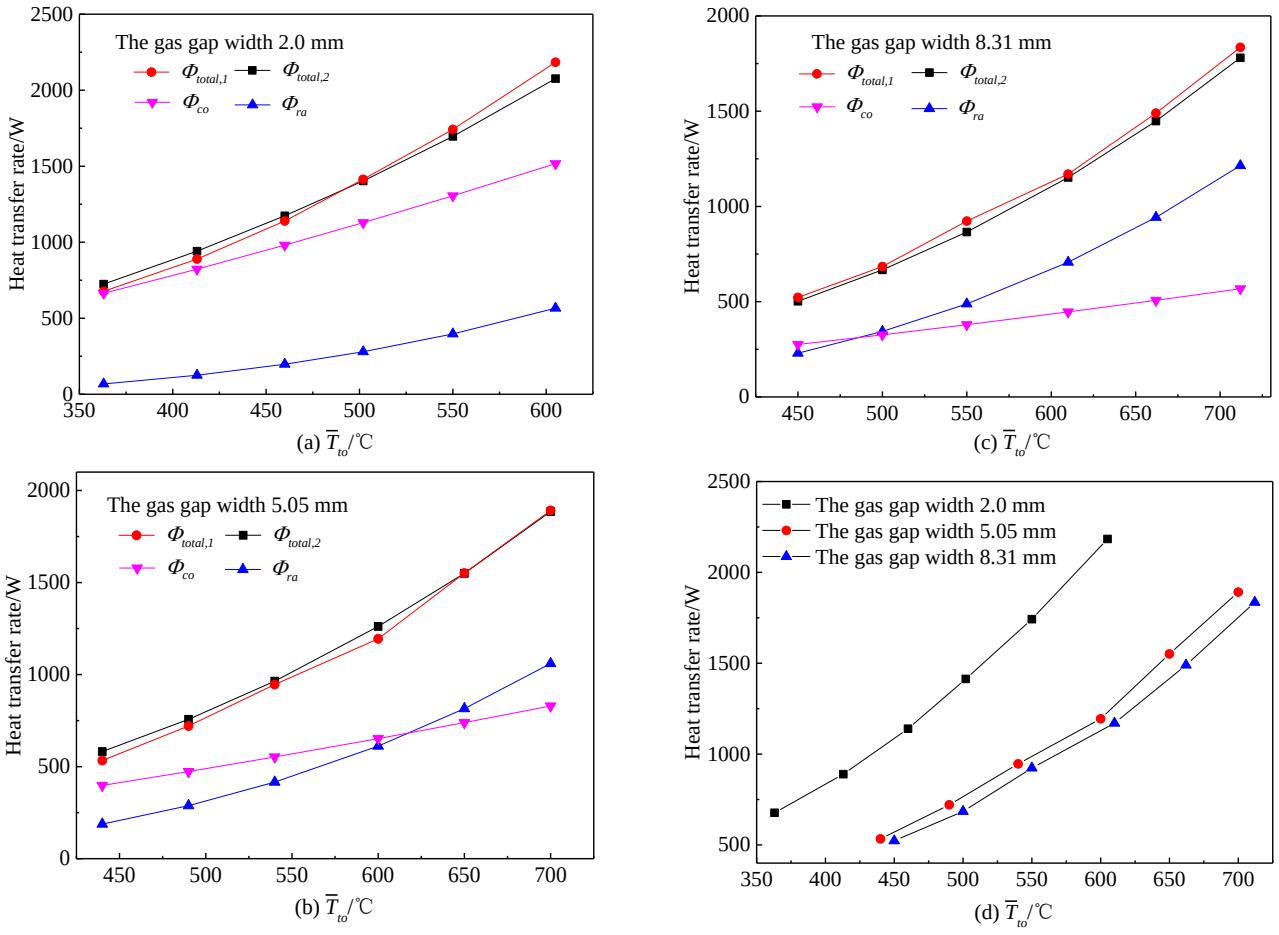

Fig.9 The change in heat transfer rate with temperature at different gas gap widths.

4.3 Calculating the influence of the gas gap width on the heat transfer rate

The electric furnace provides high temperatures circumstance by electric heating, and transfers heat to the cooling thimble through radiation and conduction heat transfer. This type of structure introduces a problem in that the outer wall temperature of the thimble does not remain constant as thimble diameter changes. This is because the temperature of the electric furnace interior is non-uniform; the temperature close to the electric furnace wall is higher. In an actual molten salt reactor, the outer wall

temperature of the thimble changes with the temperature of the molten salt rather than the outer wall diameter. Therefore this experiment does not exactly replicate that of the actual molten salt reactor. In this section, the outer wall temperature of the thimble is assumed to be 700°C for the calculation, a value which does not vary with thimble diameter. This assumption will better approximately an actual molten salt reactor.

According to the experimental results, the outer wall temperature of the thimble is approximately 700°C when the furnace temperature is 800°C. In that situation, the system pressure and wall temperature are both stable. The two-phase flow pressure drop is calculated based on the homogeneous flow model. To calculate the heat transfer rate more accurately, the heating section of the bayonet is divided into five parts. The temperature of each part is considered to be uniform. Considering that the heating above T_{bo4} represents saturated boiling and heating below T_{bo4} represents subcooled boiling, different forms of the Chen formulae are applied. Moreover, in the calculation process, the equivalent diameter of the rising channel is larger than 6.0 mm, and this channel is considered to be conventional channel by Mehendale *et al* and Kandlikar *et al* [16, 17].

This section analyzes the influence of gas gap width on the heat transfer rate by the self-compiling program. The calculation results are shown in Fig. 10.

As shown in Fig. 10 (a), when the diameter of the thimble is kept at 38 mm and the diameter of the bayonet is changed, the radiation heat transfer rate and the conduction heat transfer rate will decrease together with the increase in gas gap width. It can be concluded that above that the change in conduction heat transfer rate caused by the change in the gas gap width is more significant than the change in the radiation heat transfer rate caused by the change in the heat transfer area. The change of total heat transfer rate has the same tendency as the change of conduction heat transfer rate.

As shown in Fig. 10 (b), when the diameter of the bayonet is kept at 25.6 mm and the diameter of the thimble is changed, increasing the gas gap width increases the radiation heat transfer area causing the radiation heat transfer rate to increase. The variation tendency of the radiation heat transfer rate is slightly different than that of Fig. 10 (a). At the same time, another result of increasing the gas gap width is that it will increase the thermal resistance, which will result in a decrease in the conduction heat transfer rate. The total heat transfer rate has the same variation tendency as that of the conduction heat transfer rate. Moreover, when the gas gap width is very narrow, the heat transfer rate decreases sharply with the increase in the gas gap width. The reason for this is when the gas gap width is narrow, d_{ti} is close to d_{bo}, and the increase of d_{ti} will make the conduction thermal resistance increase sharply in the beginning, the tendency of which corresponds to a logarithm function which is shown in the Eq. (13).

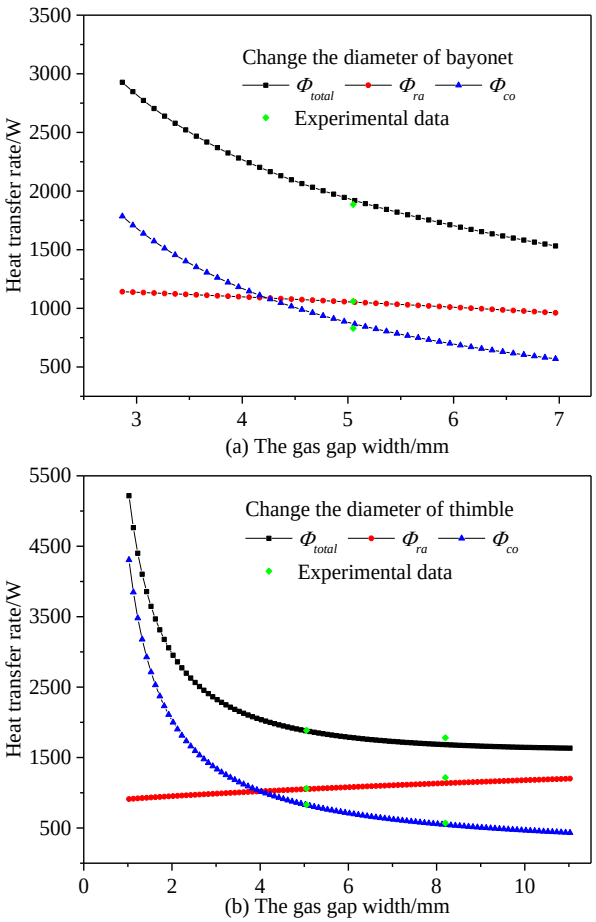

Fig. 10 The influence of the gas gap width on the heat transfer rate.

It can be seen from Fig. 10 that the calculation results correspond closely with the experimental results except that the experimental results are slightly higher than the calculation results for a gas gap width of 8.31

mm. This occurs because there is a temperature gradient in the radial direction of the furnace. The actual values of $\overline{T}_{to}$ are approximately 700°C and 712°C when the gas gap widths are 5.05 mm and 8.31 mm, respectively. However, Fig. 10 is obtained based on the assumption that $\overline{T}_{to}$ is 700°C because we cannot make the assumption that $\overline{T}_{to}$ is 700°C and 712°C simultaneously in the calculation program. Even so, we can still conclude that the calculation results correspond well to the experimental results from the figure.

It can be seen from the calculation results above that the gas gap width has a large influence on the heat transfer rate. With the increase in the gas gap width from 1.0 mm to 11.0 mm, the heat transfer rate decreases from 5.2 kW to 1.6 kW. This conclusion is different from the conclusion drawn by Lu Sun *et al* [18], which says that the gas gap width in the bayonet of cooling thimbles has little effect on the heat transfer rate. In theory, we can attempt to decrease the gas gap width in order to increase the heat transfer rate. However, when the gas gap width is very narrow, it is very difficult to arrange the thermocouples on the pipe wall. This long, thin structure makes it very difficult to insert the bayonet into the thimble and ensure that the bayonet is exactly in the center of the thimble. Moreover, it would be very expensive to manufacture and install such elaborate cooling thimbles. There is no need to make the gas gap width very thin, we can simply increase the number of cooling thimbles in the actual molten salt reactors to increase the heat removal capacity.

4.4 Uncertainty analysis

There are two kinds of uncertainty in theory. The first category of uncertainty is concerned with repeated parameter measurements, which are generally obtained through statistics analysis. The second category of uncertainty is concerned with the systemic error of measuring instruments or environmental and human-introduced error. There is no first category uncertainty in the measurement process of the heat transfer rate, since the parameters were all measured with a single measurement. The uncertainties in the relevant parameters can be calculated based on the Kline-McClintock method [19].

In this experiment, the heat transfer rate of the cooling thimble is measured by Eq. (15) and there is some systemic error introduced by measuring instruments such as thermocouples and pressure transmitters. The thermocouples are calibrated to have an accuracy of 0.5°C, the accuracy of pressure transmitters is given by the manufacturer with calibration certificates and is confirmed to be 0.1%. There are also some human-introduced errors in the measuring process. The measurement accuracy of the condensed water height is 0.5 mm, and the accuracy of recording the time τ using a stopwatch is 0.5s.

Taking the measuring time and condensed water height into consideration, the uncertainty in the heat transfer rate can be calculated by Eq. (16) and Eq. (17). Bringing the values into the equation the uncertainty in the heat transfer rate is obtained as 0.39%.

$$\begin{cases} \dfrac{\partial \ln \Phi}{\partial D_{cw}} = \dfrac{2}{D_{cw}} \\ \dfrac{\partial \ln \Phi}{\partial L_{cw}} = \dfrac{1}{L_{cw}} \\ \dfrac{\partial \ln \Phi}{\partial T} = \dfrac{\partial \ln\left(H''_{sat} - H'_{sat}\right)}{\partial T} = \dfrac{1}{H''_{sat} - H'_{sat}}\left(\dfrac{\partial H''_{sat}}{\partial T} - \dfrac{\partial H'_{sat}}{\partial T}\right) = \dfrac{1}{H''_{sat} - H'_{sat}}\left(\dfrac{H''_{sat,1} - H''_{sat,2}}{T''_1 - T''_2} - \dfrac{H'_{sat,1} - H'_{sat,2}}{T'_1 - T'_2}\right) \\ \dfrac{\partial \ln \Phi}{\partial \tau} = -\dfrac{1}{\tau} \\ \dfrac{\partial \ln \Phi}{\partial \upsilon'} = -\dfrac{1}{\upsilon'} \cdot \dfrac{\partial \upsilon'}{\partial T} = -\dfrac{1}{\upsilon'} \cdot \dfrac{\upsilon'_1 - \upsilon'_2}{T'_1 - T'_2} \end{cases} \quad (16)$$

$$\frac{\Delta \Phi}{\Phi}=\sqrt{\left(\frac{\partial \ln \Phi}{\partial D_{cw}}\right)^2\cdot \delta D_{cw}^2+\left(\frac{\partial \ln \Phi}{\partial L_{cw}}\right)^2\cdot \delta L_{cw}^2+\left(\frac{\partial \ln \Phi}{\partial T}\right)^2\cdot \delta T^2+\left(\frac{\partial \ln \Phi}{\partial \tau}\right)^2\cdot \delta \tau^2+\left(\frac{\partial \ln \Phi}{\partial \upsilon'}\right)^2\cdot (\delta \upsilon')^2}$$
$$=\sqrt{4\cdot\left(\frac{\delta D_{cw}}{D_{cw}}\right)^2+\left(\frac{\delta L_{cw}}{L_{cw}}\right)^2+\left[\left(\frac{H''_{sat,1}-H''_{sat,2}}{T''_1-T''_2}-\frac{H'_{sat,1}-H'_{sat,2}}{T'_1-T'_2}\right)\cdot\frac{\delta T}{H''-H'}\right]^2+\left(\frac{\delta \tau}{\tau}\right)^2+\left(\frac{\delta t}{\upsilon'}\cdot\frac{\upsilon'_1-\upsilon'_2}{T'_1-T'_2}\right)^2} \quad (17)$$

5 Conclusion

1. There is little difference between the two methods of obtaining the heat transfer rate, with an average difference of approximately 5%. At the same thimble outer wall temperature, the heat transfer rate at a gas gap width of 5.05 mm is similar to the heat transfer rate at a gas gap width of 8.31 mm, with an average difference of approximately 10%. However, the heat transfer rate at a gas gap width of 2.0 mm is much larger, the heat transfer rate increases by 95% when the gas gap width decreases from 5.05 mm to 2.0 mm, which demonstrates that the heat transfer rate can decrease significantly with an increase in gas gap width when the gas gap width is narrow. However, the heat transfer rate hardly changes when the gas gap width increases to a certain degree.
2. The calculation results indicate that the gas gap width has a large influence on the heat transfer rate. With the increase in the gas gap width from 1.0 mm to 11.0 mm, the heat transfer rate decreases by 70%, from 5.2 kW to 1.6 kW. The conduction heat transfer rate decreases by 90%, from 4.3 kW to 0.432 kW, and the radiation heat transfer rate increases by 32%, from 0.91 kW to 1.2 kW. This indicates that the influence of changing the gas gap width on the conduction heat transfer rate is much larger than that on the radiation heat transfer rate. We can attempt to decrease the gas gap width in order to increase the heat transfer rate in theory, but we should also take the fabrication difficulty and economics into consideration.

Acknowledgments

This work is conducted with financial support from the National Natural Science Foundations of China (Grant No. 11475048) and support of Fundamental Science on Nuclear Safety and Simulation Technology Laboratory, Harbin Engineering University, China.

References

[1] HOLCOMB, D. E., and CETINER, S. M.: An Overview of Liquid-Fluoride-Salt Heat Transport Systems [J]. ORNL/tm. 2010.

[2] ROBERTSON, R. C.: MSRE DESIGN AND OPERATIONS REPORT. PART I. DESCRIPTION OF REACTOR DESIGN [J]. 1965.

[3] HAUBENREICH, P. N., ENGEL, J. R., and PRINCE, B. E., *et al*.: MSRE DESIGN AND OPERATIONS REPORT. PART III. NUCLEAR ANALYSIS [J]. Absorption. 1964.

[4] TALLACKSON, T.: MSRE DESIGN AND OPERATIONS REPORT. PART IIA. NUCLEAR AND PROCESS INSTRUMENTATION [J]. 1968.

[5] HOLCOMB, D. E., FLANAGAN, G. F., and MAYS, G. T., *et al*.: Fluoride Salt-Cooled High-Temperature Reactor Technology Development and Demonstration Roadmap [J]. Office of Scientific & Technical Information Technical Reports. 2013.

[6] ISHIGURO, T., VAN ROOIJEN, W.F.G., and SHIMAZU, Y., *et al*.: Design of a passive residual heat removal system for the FUJI-233Um molten salt reactor system [J]. Annals of Nuclear Energy. 2014: 398-407.

[7] IGNATIEV, V., FEYNBERG, O., and GNIDOI, I., *et al*.: Progress in development of Li, Be, Na/F molten salt actinide recycler & transmuter concept [J]. 2007.

[8] MERLE-LUCOTTE, E., HEUER, D., and ALLIBERT, M., *et al*.: Launching the thorium fuel cycle with the Molten Salt Fast Reactor [J]. International Congress on Advances in Nuclear Power Plants. 2011.

[9] IWAMURA, T., MURAO, Y., and ARAYA, F., *et al*.: A concept and safety characteristics of JAERI passive safety reactor (JPSR) [J]. Progress in Nuclear Energy. 1995, 29(95): 397-404.

[10] JUHN, P. E., KUPITZ, J., and CLEVELAND, J., *et al*.: IAEA activities on passive safety systems and overview of international development ☆ [J]. Nuclear Engineering & Design. 2000, 201(1): 41-59.

[11] ZHANG, Y. P., QIU, S. Z., and SU, G. H., *et al*.: Analysis of safety margin of in-vessel retention for AP1000[J]. Nuclear Engineering & Design. 2010, 240(8): 2023-2033.

[12] WANG, C., GUO, Z., and ZHANG, D., *et al*.: Transient behavior of the sodium–potassium alloy heat pipe in passive residual heat removal system of molten salt reactor [J]. Progress in Nuclear Energy. 2013, 68: 142-152.

LABORATORY, O.R.N.: Molten-Salt Reactor Program Semiannual Progress Report, July 31, 1963 [J]. 1963.

[13] CHEN, J. C.: Correlation for Boiling Heat Transfer to Saturated Fluids in Convective Flow [J]. Industrial & Engineering Chemistry Process Des... 1966, 5(3): 322-329.

[14] YAN, J., BI Q., and LIU Z., *et al*.: Subcooled flow boiling heat transfer of water in a circular tube under high heat fluxes and high mass fluxes [J]. Fusion Engineering & Design. 2015, 100: 406-418.

[15] MEHENDALE, S. S., JACOBI, A. M., and SHAH, R. K.: Fluid Flow and Heat Transfer at Micro and Meso-Scales With Application to Heat Exchanger Design [J]. Applied Mechanics Reviews. 2000, 53(7): 175-193.

[16] KANDLIKAR, S.G.: Fundamental issues related to flow boiling in minichannels and microchannels [J]. Experimental Thermal & Fluid Science. 2002, 26(2–4): 389-407.

[17] SUN, L., SUN, L., and YAN, C., *et al*.: Conceptual design and analysis of a passive residual heat removal system for a 10MW molten salt reactor experiment [J]. Progress in Nuclear Energy. 2014, 70(1): 149-158.

[18] KLINE, S.J., and MCCLINTOCK, F.A.: Describing Uncertainties in Single-Sample Experiments [J]. 1953.